

Energy Partition and Attenuation of Regional Phases by Random Free Surface

by Li-Yun Fu, Ru-Shan Wu, and Michel Campillo

Abstract The earth's topography is generally rough at various scales. Numerical simulation techniques are used in this study to investigate the energy attenuation of regional phases across a randomly rough topography. We demonstrate a clear statistical correlation of the distance-dependent energy distribution with path topographic properties parameterized by the surface correlation length a and the surface root-mean-square height σ . Numerical experiments show that interference of randomly scattered waves by topography can cause regional wave amplitude undergoing strong variations. The topographic-scattering-driven energy distribution over a long distance is usually characteristic of an attenuation trend on the long distance scale, accompanied by amplitude fluctuations on the smaller distance scale. Total energy attenuation can be divided into large-scale and small-scale components that are correlated, respectively, in quite different manners, with along-path topographic statistics. On the one hand, the small-scale energy component is strongly related to the near-receiver topographic geometry. It has a striking similarity to the corresponding topographic curve. The spatial fluctuation of the small-scale component depends on a , whereas its amplitude amplification/deamplification is mainly related to σ , wavelength, and local incident angles. On the other hand, the large-scale component of energy curve, described by a scattering Q , demonstrates a scale-dependent relation with topographic statistics. A two-step analysis method is presented to evaluate the mantle leakage loss due to topographic scattering. The resultant topographic scattering Q is comparable with some observations with Q measured as a mean value in the crust. In summary, the study suggests the concept that topographic scattering might be a powerful mechanism to attenuate regional waves.

Introduction

Rugged topography and its statistical characteristics, as traces of the past tectonic processes and physiographic evolution of the earth surface, have a significant influence on the data interpretation of ground motion and regional phases. The free-surface stochastic fluctuations of all scales function as a highly lateral heterogeneity of the crust, with wavelength-scale variations in wave scattering existing at different levels of roughness of the earth surface in different tectonic regions. Forward and back multiple scatterings by rugged topographies along the path of regional phases tend to remove some energy from the guided waves and cause the decay of wave-guide energy (Fu and Wu, 2001). At present, however, we still lack a convincing explanation for attribution of the topographic scattering to the attenuation of regional phases. In this study, more quantitative assessment of the topographic effects will be conducted by studying the close relation of the statistical characteristics of random free surface and its scattering attenuation to regional waves.

With the extensive publications in seismology, the scat-

tering effects from small-scale and large-scale crustal heterogeneities on seismic-wave propagation are well explained. Wave scattering from rough surface has been another major subject of a large number of research articles, both theoretical and experimental. The effects of the near-source topographic scattering were estimated from teleseismic P waves propagating through a 2D surface topography (McLaughlin and Jih, 1988) and a 3D topographic scarp (Frankel and Leith, 1992). In comparison with the near-source topographic effects, regional phases are more affected by path topographic properties and the near-receiver topographic geometry. Bouchon *et al.* (1996) gave a comprehensive review of studies of the topographic effects on seismic waves. They concluded that the topographic scattering is an important source of seismic coda and the large amplification of ground motion often occurs near the top of a hill or mountain along the crest of a ridge. As illustrated with simple model tests (Jih, 1996), L_g propagation is not affected by a moderate free-surface topography alone as much as other types of

heterogeneity because the surface topography variations are generally small relative to the crustal thickness. It is very different from the cause of Rg for which the rough free surface is shown to be a strong scatterer because Rg energy is confined in the uppermost layer. In comparison with the crustal thickness, the effects of topographic scattering on Lg or Rg may be more related to the ratio of scatterer size to wavelength. We conducted numerical modeling tests with from simple to complex models and found that a moderate topography generally produces more forward coherent scattering and less backscattering, whereas a rugged topography can form strong forward diffuse scattering and back multi-scattering. The topographic scattering is also relative to the incident angle at which Rg is different from Lg waves. Lg waves are multiple reflected within the crust and incident on the Moho at an angle more grazing than the critical angle.

The observations of path effects on Lg propagation in different geological and geophysical environments have shown some evidence for the sensitivity of Lg to topographic properties. Baumgardt (1990) observed that the near-surface sediment-thickness variations caused by the surface elevations appear to be more important in attenuating Lg propagation than do the crustal thickness variations. Recent studies have shown that regional phase amplitude ratios seem to correlate strongly with the along-path topographic statistics in the Western United States (Zhang *et al.*, 1996), western China (Fan and Lay, 1998; Hartse *et al.*, 1998), Alibek, Turkmenistan (ABKT) (Rodgers *et al.*, 1997), and Eurasia (Zhang and Lay, 1994), especially for the components at frequencies greater than 3 Hz in some paths in central Eurasia (Baumgardt and Der, 1994). On the one hand, some plateaus consist of a series of mountain belts in close proximity to each other, which presents a small-scale varying rough topography ranging a great extent. The topography can progressively scatter and attenuate regional phases, depending on its statistical characteristics. For example Lg propagates efficiently across Turkey, Iran, and adjacent regions, but the Lg waves that cross the Turkish and Iranian plateaus are weak and have relatively long predominant periods of about 2–5 sec (Kadinsky-Cade *et al.*, 1981). On the other hand, the large-scale varying topography as a manifestation of the varying crustal thickness in some continental areas has been observed to block Lg phases, as for the Tibetan plateau (Ruzaikin *et al.*, 1977; Ni and Barazangi, 1983) and near the Alpine Mountains (Campillo *et al.*, 1993). Investigations by McNamara *et al.*, (1996) showed that for paths entirely within the Tibetan Plateau, Lg propagates efficiently, whereas for events located outside of the Plateau, Lg is either absent or severely diminished when across both the Himalayan and Kunlun ranges. That is, the margins of the Plateau weaken Lg transmission. Theoretical studies of Lg propagation conducted by Kennett (1986), Campillo (1987), and Maupin (1989) confirmed that the large-scale lateral changes in crustal discontinuities and crustal thickness strongly affect regional phases. The above review of previous studies suggests that scattering by dra-

matic lateral variations of the topography-Moho large-scale structures combined with the small-scale rough topography may play a prominent role among the causes for the regional wave attenuation and blockage. So far, however, the clear delineation, even a preliminary appraisal of topographic effects on regional phases, has not been given because of the complexity of the problem.

In this study, the boundary-element (BE) numerical technique is modified for long-distance propagation simulation in order to explore the spatial attenuation and energy partition of regional phases across a randomly rough topography. We seek to characterize the correlation of the distance-dependent energy distribution of regional phases with path properties parameterized in terms of topographic roughness. This correction may help us define the contribution of topographic scattering to regional wave attenuation. We first briefly summarize the numerical simulation technique used in this study, demonstrate a clear statistical correlation of topographic scattering characteristics with along-path topographic statistics, and finally, discuss the Lg -energy attenuation by random topography. A numerical experiment shows that interference of randomly scattered waves by topography can cause regional wave amplitude undergoing strong variations. Total energy attenuation by topographic scattering is clearly divided into large-scale and small-scale components correlated respectively in quite different manners with along-path topographic statistics. This study provides insight into the calibration of regional discriminants for path effects in terms of observable surface topography.

Methodology

Lg energy consists of shear waves that are reflected supercritically between the topography and the Moho and therefore trapped in the crust. Four problems associated with the Lg -propagation simulation have been recognized: large-scale lateral crustal variations, small-scale heterogeneities in the crust, computations with higher frequencies, and far regional propagation distances. Analytical solutions can give insight into wave-propagation phenomena but are only applicable to very simple models. Complex geological models can be generally solved by finite-difference and finite-element methods that, however, are time-consuming and also lack an analytical guideline for propagation phenomena. Several efficient semianalytical, seminumerical methods have been designed to simulate the Lg propagation, for instance, the discrete wavenumber decomposition (Bouchon, 1982), the coupled mode method (Kennett, 1984, 1998), the global generalized reflection/transmission matrices method (Chen, 1995), and the BE method (Gibson and Campillo, 1994). These methods, however, are restricted to lower frequencies for Lg simulation at regional distances. To reduce computation time for Lg simulation, Wu *et al.* (1996, 2000a) introduce a one-way, half-space generalized screen propagator (GSP) for modeling the main characteristics of Lg in smoothly varying heterogeneous crustal waveguides. The

method has been extended to handle mild topographies (Wu *et al.*, 1999). A hybrid method of BE and GSP for a 2D *SH* problem (Fu and Wu, 2001) has been developed to study the combined effects of both rough topography and heterogeneous media on *Lg* propagation. In the hybrid scheme, the time-consuming BE method can be used to handle all scatterings reverberated inside the rugged free-surface structure, whereas the large volume of moderately heterogeneous media can be modeled by the GSP method.

In this study, we use the BE method to investigate the topographic scattering effects on regional wave propagation. The method can handle multiple scatterings by rough topographies. The traction-free condition for rugged free surface is easy and natural to treat in an accurate and stable manner. The direct BE method has been widely used due to the explicit meaning of the unknowns in the formulation (e.g., Wong and Jennings, 1975; Dravinski, 1982; Fu and Mu, 1994), whereas the indirect method formulates problems in terms of force or force moment boundary densities (e.g., Sanchez-Sesma and Campillo, 1991). In this section, the direct BE method and its modification for long-distance propagation are briefly described. Consider 2D steady state *SH*-wave propagation in a homogenous region Ω_0 bounded by a rough free surface Γ_0 and an irregular Moho interface Γ_1 . Figure 1 depicts the geometry of the problem. The antiplane displacement $u(\mathbf{r})$ at a location \mathbf{r} in the domain Ω_0 satisfies the steady-state boundary integral equation

$$C(\mathbf{r})u(\mathbf{r}) + \int_{\Gamma} \left[u(\mathbf{r}') \frac{\partial}{\partial n} G(\mathbf{r}, \mathbf{r}') - G(\mathbf{r}, \mathbf{r}') \frac{\partial}{\partial n} u(\mathbf{r}') \right] d\mathbf{r}' = u^0(\mathbf{r}), \quad (1)$$

where the boundary $\Gamma = \Gamma_0 + \Gamma_1$, the coefficient $C(\mathbf{r})$ is equal either to 1.0 for the location \mathbf{r} inside Ω_0 or depends on the local geometry at \mathbf{r} for the location \mathbf{r} on Γ , $G(\mathbf{r}, \mathbf{r}')$ is the free-space Green's function for the homogeneous media, $\partial/\partial n$ denotes differentiation with respect to the outward normal of the boundary Γ , and $u^0(\mathbf{r})$ is incident field. For the presence of a point source located at \mathbf{r}_0 inside Ω_0 , it can be expressed by $u^0(\mathbf{r}) = S(\omega)G(\mathbf{r}, \mathbf{r}_0)$, where $S(\omega)$ is the source spectrum. Applied to topography with the traction-free condition, equation (1) is reduced to

$$C(\mathbf{r})u(\mathbf{r}) + \int_{\Gamma_0} u(\mathbf{r}') \frac{\partial}{\partial n} G(\mathbf{r}, \mathbf{r}') d\mathbf{r}' + \int_{\Gamma_1} \left[u(\mathbf{r}') \frac{\partial}{\partial n} G(\mathbf{r}, \mathbf{r}') - G(\mathbf{r}, \mathbf{r}') \frac{\partial}{\partial n} u(\mathbf{r}') \right] d\mathbf{r}' = u^0(\mathbf{r}). \quad (2)$$

For *SH*-wave propagation in Ω_1 bounded by the Moho Γ_1 and an infinite boundary, we have the boundary integral equation with the following form

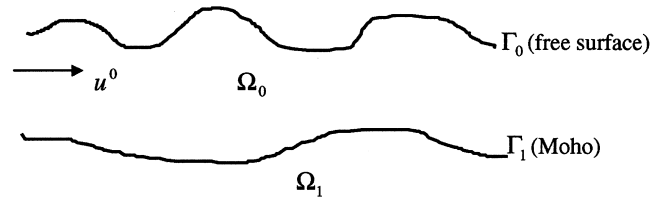


Figure 1. Geometry of the problem. The free surface and Moho interface have arbitrary shape.

$$C(\mathbf{r})u(\mathbf{r}) + \int_{\Gamma_1} u(\mathbf{r}') \frac{\partial}{\partial n} G(\mathbf{r}, \mathbf{r}') d\mathbf{r}' = \int_{\Gamma_1} G(\mathbf{r}, \mathbf{r}') \frac{\partial}{\partial n} u(\mathbf{r}') d\mathbf{r}'. \quad (3)$$

The numerical implementation of the BE method is performed in the frequency domain. Because the Green's integral equation formulations enjoy a unique advantage in defining domains extending to infinity, the exterior ends of the interfaces in the model can be handled using an infinite boundary element absorbing boundary technique (Fu and Wu, 2000). Equation (3) is approximated by boundary elements respectively in each Ω_0 and Ω_1 and transformed into a simultaneous system of linear equations using the following boundary conditions of continuity for displacements and stresses across the Moho interface:

$$\begin{cases} u_1 = u_2 \\ \mu_1 \frac{\partial u_1}{\partial n} = \mu_2 \frac{\partial u_2}{\partial n} \end{cases}, \quad (4)$$

where μ is the shear modulus, u_1 and u_2 are the displacements, above and below the Moho interface, respectively. The boundary integral representation in equation (3) makes it convenient to compute the observation field scattered from either the topography or the Moho. We can also divide the model into several subregions. The composite observation fields can be represented as a summation of integrals over the subregions, by which we can split up the observation fields into different parts that are contributed from different subregions of the model, particularly separating topographic scattering from the overall observation field in the crustal wave guide.

The BE formulations generally give rise to a large system of equations for *Lg* simulation. Because the considerable amount of matrix operations are involved and the matrix for each frequency component must be inverted, the BE method is computationally intensive at high frequencies. The numerical burden of this method can be circumvented with the use of (1) a variable element dimension technique (Fu, 1996), in which the element dimension for each frequency is computed according to the medium velocity and the frequency and the model is then automatically discretized; and (2) a threshold criterion (Bouchon *et al.*, 1995) to invalidate

very small entries in the coefficient matrix in terms of the significant spatial decay of Green's functions at far regional propagation distances.

For an event at far regional distance up to several thousand kilometers, the BE method can be used section by section, with the output of previous section as the input to the next section in order to complete the entire crustal wave guide computation. A boundary connection technique (Fu and Wu, 2001) has been developed to couple the fields calculated in two adjoining sections. The division of sections is based on the topographic features. The purpose is to minimize the possible multiple backscattering between sections so that the transmission between sections can be treated by one-way approximation. This section-by-section approach to long regional wave guides leads to significant computational savings in time and memory compared with taking the whole wave guide as one section. It becomes a computationally viable technique for practical *Lg* modeling.

Trifunac's half-space semicircular canyon topography of radius a_0 is used to test the accuracy of the computation program described previously. Trifunac (1973) gave the exact solution in the frequency domain. Figure 2 shows the comparison with good agreement between our results and analytical solutions for 60° incident *SH* wave and for various normalized frequencies η defined as $\eta = 2a_0/\lambda$, where λ is the wavelength. We can see some minor departures because of the numerical approximation of element length to the arc of the semicircular canyon. The second example shows, by

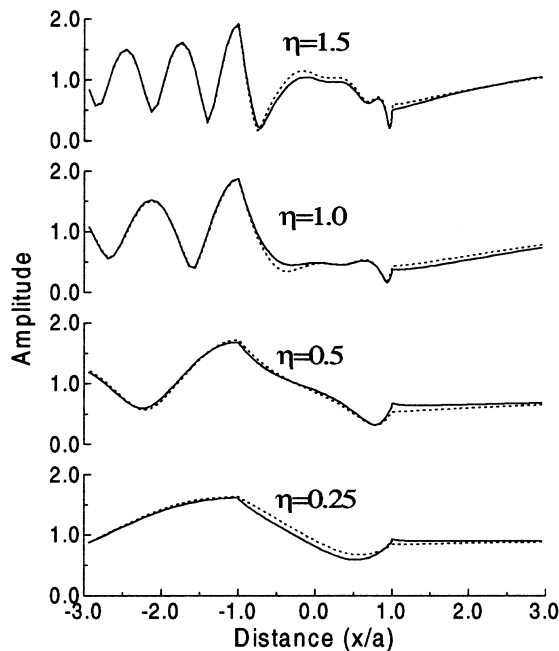


Figure 2. Comparison of results to exact solution for a semicircular canyon topography with 60° incident *SH* wave for various dimensionless frequencies η . The solid lines denote our results, and the dotted lines denote the exact solutions (Trifunac, 1973).

intuitional snapshots, the significant impact of rough random free surface on the seismic response. The medium considered consists of a homogeneous crustal wave guide, 200 km long and 20 km thick, overlaying a flat mantle half-space. The root-mean-square (RMS) height of the random topography is 2.5 km. The point source (Gaussian derivative function) is located on the left boundary at 2.0-km depth. The snapshots shown in Figure 3, calculated at 25, 35, and 50 sec, respectively, demonstrate the development of mantle wave and head wave, as well as the formation of crustal-guided waves as repetitive reflections at both the free surface and the Moho. The *SH* waves incident upon the free surface and the Moho at an oblique angle can be divided into two systems, one set off at the free surface and another off at the Moho. These two systems of waves bounce back and forth between the free surface and the Moho and will be confined in the wave guide at a postcritical angle. These snapshots demonstrate a clear onset with maximum amplitude in the consecutive wavefronts. The bundle of repetitive reflections, however, exhibits strong apparent attenuation due to the scattering by rough topography. The strong diffuse scattering along the topographic surface depends on the surface shape. The backscattering by local irregular topography

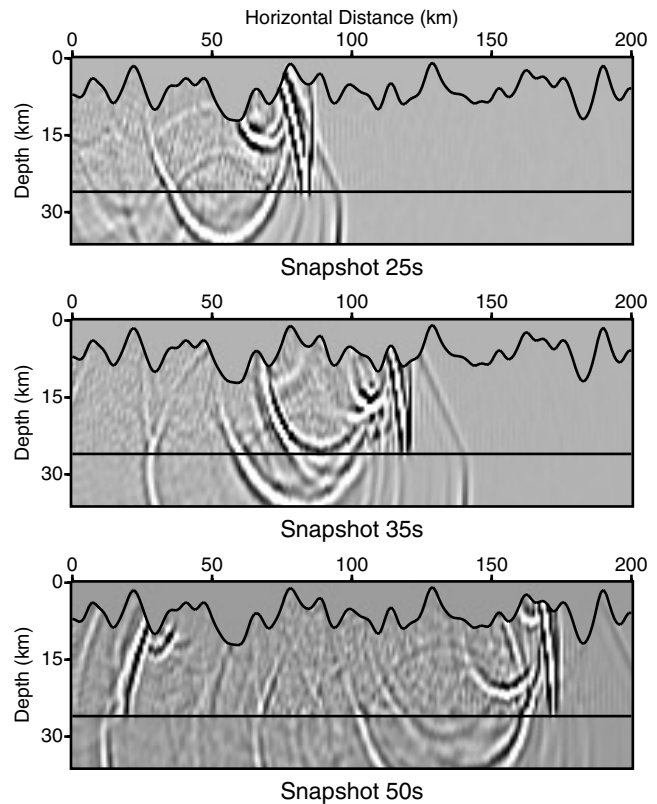


Figure 3. Snapshots of *SH* waves passing a homogeneous wave guide with a randomly rough free surface of the surface rms height $\sigma = 2.5$ km. The source depth is 2.0 km, and the wave-guide thickness is 20 km. Seismograms are computed in the frequency range of 0–2 Hz.

tends to remove much energy from the guided wave, with a large percentage leaking into the mantle and the rest contributed to the coda along the wave train as time progresses. In summary, the rough topography can increase energy diffusion and complexity of regional wave propagation. It can be expected that a rough surface topography with its scale length close to the dominant wavelength will be very efficient in attenuating regional waves.

Studies of the Effect Pattern of Along-Path Topographic Statistics on Regional Wave Propagation

Statistical Description of Rough Surfaces

The earth's surface is generally rough with features exhibiting a random heterogeneity on a wide variety of scales. These scales, relative to the wavelength of incident waves, are crucial in determining how energy is scattered. Beyond the empirical description, the geometrical heterogeneities of surface topography can be characterized by different statistical parameters. Assuming the surface height distribution function is $h(\mathbf{r})$, where h is the height of the surface from the reference surface and \mathbf{r} is the position of points on the reference surface. The rms height of the surface $h(\mathbf{r})$ is then defined as the standard deviation $\sigma = \sqrt{\langle h^2 \rangle}$ where $\langle \dots \rangle$ denotes the process of spatial averaging across the surface. In this study, the surface is assumed spatially stationary and ergodic, with its $h(\mathbf{r})$ being zero mean (i.e., $\langle h \rangle = 0$).

The roughness of the random surface height $h(\mathbf{r})$ is defined by its second moment, that is, the surface correlation function, defined as $C(\mathbf{r}) = \langle h(\mathbf{r}')h(\mathbf{r}' + \mathbf{r}) \rangle / \sigma^2$, where σ^2 is simply the variance at a lag of $\mathbf{r} = 0$ and used to normalize the autocovariance $\langle h(\mathbf{r}')h(\mathbf{r}' + \mathbf{r}) \rangle$. The normalized autocorrelation function has the property that $C(0) = 1$, decaying to zero as \mathbf{r} increases. The shape of this decay depends on the type of the surface, and the decay rate depends on the correlation length, that is, the distance beyond which the surface profile becomes uncorrelated. The Fourier transform of the autocorrelation function is the roughness spectrum that measures the height variation with spatial frequency for a random surface. Much of the literature on wave scattering from rough surface assumes that surface correlation functions are Gaussian given by $\exp(-|\mathbf{r}|^2/a^2)$ or exponential by $\exp(-|\mathbf{r}|/a)$, where a is the correlation length, a distance over which the correlation function falls by $1/e$. In practice, rough surfaces often possess more than one correlation length, especially for a long propagation distance over which more than one geological process is responsible for forming the path surface. In our computations, we use a standard crustal waveguide with $V_{\text{crust}} = 3.5 \text{ km s}^{-1}$, $\rho_{\text{crust}} = 2.8 \text{ g cm}^{-3}$, $V_{\text{mantle}} = 4.5 \text{ km s}^{-1}$, and $\rho_{\text{mantle}} = 3.2 \text{ g cm}^{-3}$, the Moho interface at 32-km depth, and the source at 2.0-km depth. The critical distance of crustal wave is around 90 km for this wave guide. We only concentrate on the surface rms height σ and the surface correlation length a with an expo-

ponential correlation function for the analysis of energy distribution of regional waves.

Effects by the Surface RMS Height σ

We first investigate how the surface rms height affects wave scattering behavior and energy partition. Figure 4 shows two random topographies of the same correlation length ($a = 4.0 \text{ km}$) but different surface rms heights, one with $\sigma = 2.5 \text{ km}$ (thin line) and the other with $\sigma = 0.5 \text{ km}$ (thick line). These profiles show similar spatial variation pattern but markedly different magnitude. We use them as the surface profile, respectively, for the model in Figure 5 in the computation and compare the numerical results. The wave guide in Figure 5 has a homogeneous medium with a flat Moho interface to exclude anelastic attenuation and scattering attenuation by volume heterogeneities. Synthetic seismograms are calculated by the BE method at all discrete points along the random free surface to produce an energy profile versus distance. The energy loss of the guided wave for this homogeneous wave guide is caused only by topographic scattering, geometrical attenuation, and leakage to the mantle.

Figure 6 shows a comparison of total energy attenuations for different surface profiles shown in Figure 4. Energy computation is done by a summation of all frequency components for each synthetic seismogram. The energy curves are scaled in each simulation with respect to the first receiver that is set at 0.0 km horizontally from the source. We use a

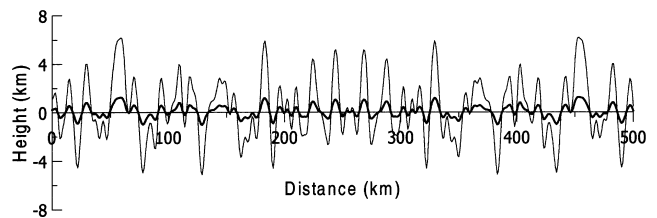


Figure 4. Randomly rough surfaces of the same correlation length ($a = 4.0 \text{ km}$) but the different surface rms height (σ) of 2.5 km (thin line) and 0.5 km (thick line).

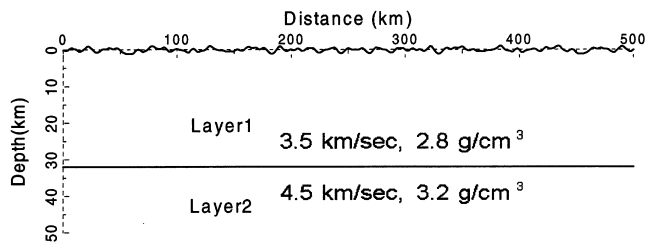


Figure 5. A 32-km-thick crust model with the random surfaces (Fig. 4) of $\sigma = 2.5 \text{ km}$ and $\sigma = 0.5 \text{ km}$, respectively. The model is used to calculate energy distributions. The source function is a Gaussian derivative with dominant frequency of 1.0 Hz and computation frequency range 0.0–2.0 Hz.

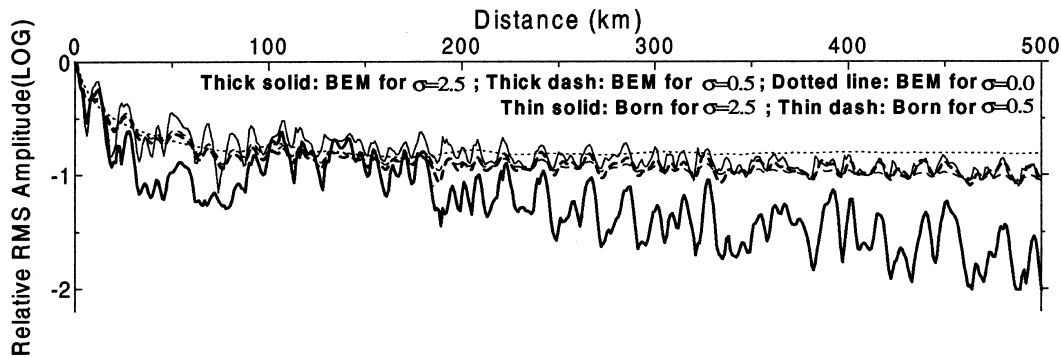


Figure 6. Total energy distribution versus distance for the model in Figure 5 with three different free surfaces: $\sigma = 2.5$ km (solid line), $\sigma = 0.5$ km (dash line), and $\sigma = 0.0$ km (dotted line), calculated by the BEM (thick line) and Born approximation (thin line).

flat free surface as the reference wave guide for comparison. We see that the reference energy profile (dotted line) is kept basically constant after passing 80 km that is termed the critical distance. From the figure, we see that the energy attenuation curve for large σ (thick solid line) is much steeper and fluctuates much stronger than the curve of small σ (thick dash line). In contrast to deterministic intrinsic attenuation, the scattering apparent attenuation from random media is usually statistic in nature. That is, the trend of the exponential decay of waves over a long distance is generally accompanied by amplitude fluctuations on the smaller distance scales. From Figure 6, we see that for the small-scale fluctuations, both the patterns $\sigma = 2.5$ and $\sigma = 0.5$ share the similar variations at all bounce points because of their same local topographic structures, whereas the difference lies in magnitude. A following more-detailed discussion on the small-scale fluctuations will show that the surface rms height σ mainly affects the fluctuation amplitude of an energy profile. We see that beyond a certain distance, the trend for $\sigma = 2.5$ decreases more rapidly, with the rate of decrease depending on the value of σ . The average slope of the energy curve is largely related to the surface rms height and is used for Q estimation of scattering attenuation.

Comparisons with Perturbation Approaches

We also compare the BE method with perturbation approaches to show the extent to which the perturbation theory can be used for regional wave simulation. The thin solid and thin dash lines in Figure 6 are computed using Born approximation for the surface profiles $\sigma = 2.5$ and $\sigma = 0.5$, respectively. In our computations, the Born approximation is only applied to the displacement on the free surface, whereas the quantities (displacement and stress) on the Moho interface are obtained by solving the matrix equation associated with the crust and the mantle. For the rough surface $\sigma = 2.5$, the comparison between the thick solid (by the BE method) and the thin solid (by the Born approximation) shows that the Born approximation greatly impairs the

large-scale energy component and therefore totally underestimates energy attenuation. The Born approximation, however, shares some characteristics in the small-scale component with the BE method. For the gentle rough surface $\sigma = 0.5$, the comparison between the thick dash (by the BE method) and thin dash (by the Born approximation) demonstrates that the Born approximation can model, to a large degree, both the large-scale and small-scale components in energy. However, the error in the small-scale component increases rapidly with propagation distance, especially beyond 400 km where the energy fluctuations (by Born approximation) are obviously flattened.

Perturbation theory has been widely used in studies of wave scattering from volume heterogeneities and irregular surfaces. Kennett (1972) used Born theory approximation in the propagator matrix formalism to model layer irregularity. Perturbation methods generally assume a distant observation from scattering points, small height of topographic irregularity, and small topographic slope. Hudson *et al.* (1973) studied the accuracy of perturbation theory applied to Rayleigh-wave scattering from triangular grooved surfaces and demonstrated that the accuracy of the theory decreases as the angle of incidence increases and as the slope angle increases. It has often been suggested by numerous studies of wave scattering from irregular surfaces that perturbation theory is usually appropriate for slightly rough surfaces where the scattered field is regarded as only slightly altered by the presence of roughness. For regional phases, our study shows that perturbation theory, though ignoring the effects of multiple scattering at a rough surface, can preserve the relative variation in the small-scale energy components for a certain distance. This may be the reason that some perturbation methods can model waveforms to some degree within a certain propagation distance, even for moderate rough surfaces. However, the decreasing accuracy by flattening fluctuations is apparent as the propagation distance increases. The scattering attenuation by rough surfaces is usually measured by the average energy decay.

Backscattering Energy from Rough Surfaces

A major impetus to understand the detailed characteristics of regional waves comes with efforts to unravel seismic-coda waves. The generation of *S*-coda waves is believed to be the backscattering by the heterogeneities in the lithosphere, which feeds shear-wave energy into the later parts of the seismogram. Assuming the Born approximation, the strength of backscattering can be analytically determined by the mean square impedance perturbation of the medium (Wu, 1985). More accurate calculation can be obtained using energy transfer theory considering the effects of multiple scattering (Sato and Fehler, 2000). For rough surfaces, we lack reliable theoretical models for analytical evaluations of the separate components: forward-scattering fields, backscattering fields, and Mantle waves. The integral representation for wave scattering defined in terms of the integrals over the free surface and the Moho interface allows us to use numerical methods for computing these components, respectively.

Figure 7 shows the backscattering energy attenuation versus distance calculated from backscattered seismograms recorded at all discrete points along the random free surface. The energy at a near-source receiver comes cumulatively from the back propagation waves that are scattered from the distant parts of the path. Therefore, a common feature of these energy curves is the gradual reduction of backscattered energy at increasing distance. This leads to a general reduction of the coda amplitude along the wave train as distance progresses. It should be noted that much of the backscattered energy leaks to the mantle (see Fig. 3). As was expected, the backscattering response to the rough case $\sigma = 2.5$ is stronger than that of the gently rough case $\sigma = 0.5$. The local-irregularity-dependence of the small-scale energy component is quite complicated, particularly for the rough surface $\sigma = 2.5$, whereas the large-scale component appears relatively stable over distance. For a mild topography, the backscattered energy is weak, *Lg* energy loss is caused mainly by forward diffusion scattering with large angles, and one-way approximation to wave propagation can be applicable. The Born approximation assumes that the wavefield on to-

pography equals the incident wave, neglecting the multiple scatterings at the topography. This makes the backscattered energy even stronger in this two-way wave equation simulation. Therefore in Figure 7, we see that the Born approximation overestimates backscattered energy for both cases $\sigma = 2.5$ and $\sigma = 0.5$.

The Moho Leakage Loss

Backscattering only accounts for one part of *Lg* energy loss; another part results from the Moho leakage attenuation. The Moho leakage also removes some topography-scattered waves out of the waveguide. Wu *et al.* (2000b) conducted simulations for wave guides filled with random heterogeneities and showed that the leakage attenuation caused by large-angle foreshattering by random volume heterogeneities is significant and may become the dominant attenuation mechanism in some regions. Figure 8 shows the Moho leakage loss versus distance calculated from synthetic seismograms observed at one-wavelength depth below the Moho interface with 1.0-km apart horizontally. A glance at the figure shows a strong variation of energy leaking into the mantle arising at the crust-mantle interface up to the critical distance (<90 km). We see that beyond the critical distance, the mantle energy for all cases remains approximately the same order. This indicates that for *Lg* phases, the trapping of shear energy is quite efficient, and even in the presence of lateral heterogeneities, most of the energy can still be trapped in the crust (Kennet, 1989). From Figure 8 we see that due to the attenuation of the total crustal energy and the geometric spreading along the wave guide, the Moho energy is proportionally reduced. Because of the strong energy loss, the leaked mantle energy decreases rapidly for the case of $\sigma = 2.5$. The crosspoint between $\sigma = 2.5$ and $\sigma = 0.5$ is at the distance of 225 km. The Born approximation underestimates the Moho leakage for both cases $\sigma = 2.5$ and $\sigma = 0.5$.

Effects of the Surface Correlation Length a

As one of two essential aspects to the nature of a random rough surface, the surface correlation length a plays an im-

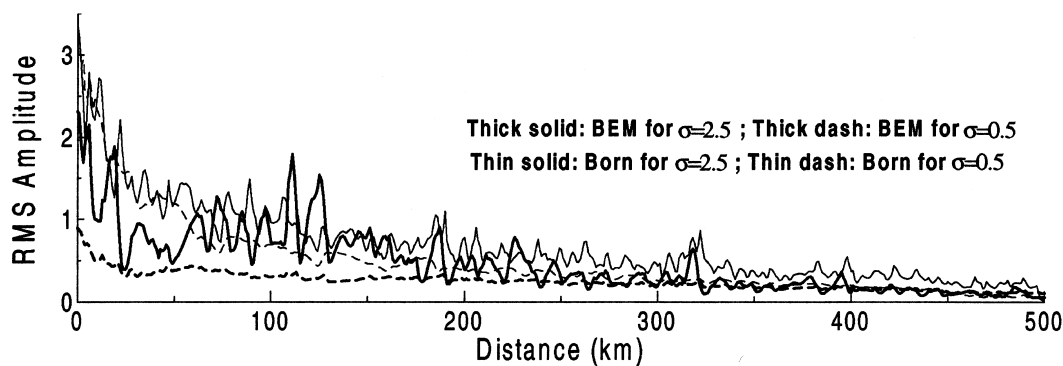


Figure 7. Backscattering-energy distribution versus distance for the model in Figure 5 with two different free surfaces: $\sigma = 2.5$ km (solid line) and $\sigma = 0.5$ km (dash line), calculated by the BEM (thick line) and Born approximation (thin line).

portant role in affecting regional wave propagation. Figure 9 shows two random topographies, at 0.5-km spacing, of the same surface rms height ($\sigma = 0.8$) but different surface correlation length, one with $a = 2.2$ (thin line) and another $a = 22$ (thick line). The value of a carries information about how far away different parts of the surface variations are still correlated each other. The interval used to discretize a random surface should be at least as small as one-tenth of the correlation length so that the full random nature of the surface can be measured (Ogilvy, 1991).

Synthetic seismograms for these two topographic profiles are calculated with a frequency range of about 0–4 Hz. Figure 10 demonstrates how the surface-correlation length

a affects the topographic scattering behavior for regional phases. These energy curves are not normalized in order to show discrepancy among the curves in absolute values. The solid line is for $a = 2.2$, the dash line is for $a = 22$, and the dotted line is for the reference waveguide. From the large-scale energy component, we see that the case of $a = 2.2$ is associated with stronger attenuation than $a = 22$. The marked difference between these two cases is in the small-scale component where the case $a = 2.2$ is characterized, against the case of $a = 22$, by a small-magnitude, short-wavelength roughness of the energy curve, as consistent with its topographic profile (see the thin curve in Fig. 9). The total energy profiles in Figure 10 are calculated includ-

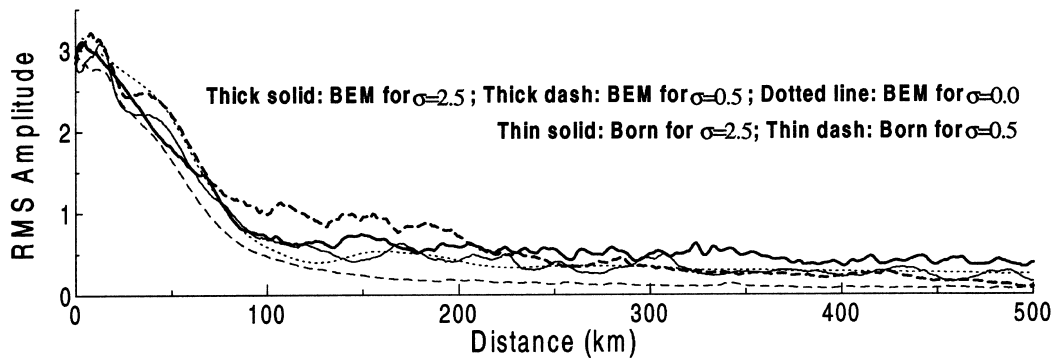


Figure 8. Moho leakage loss versus distance for the model in Figure 5 with three different free surfaces: $\sigma = 2.5$ km (solid line), $\sigma = 0.5$ km (dash line), and $\sigma = 0.0$ km (dotted line), calculated by the BEM (thick line and dotted line) and Born approximation (thin line).

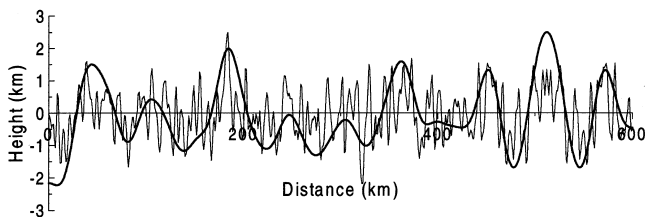


Figure 9. Rough surfaces of the same surface rms height ($\sigma = 0.8$ km) but different correlation length of 2.2 km (thin line) and 22.0 km (thick line), respectively.

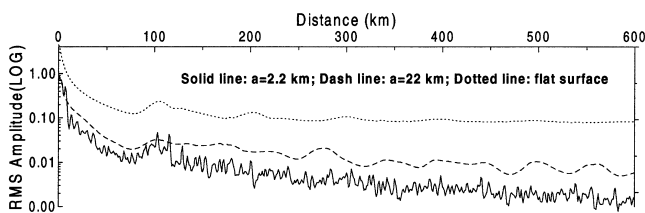


Figure 10. Total energy distribution versus distance for the wave guides with different free surfaces (see Fig. 11): $a = 2.2$ km (solid line), $a = 22$ km (dash line), and a flat surface (dotted line), calculated by the BEM in the frequency range of 0–4.0 Hz.

ing both the coherent and diffuse components of the scattered fields, where the diffuse component is scattered out of the Lg window and contributed to Lg coda. Correlations along the surface therefore affect scattering, particularly when comparable to the dominant wavelength of incident waves. The waves scattered from different parts of the surface will be strongly correlated if their phase differences are comparable with, or smaller than, the surface correlation length. In general, the diffuse field becomes small if $ka \gg 1$ (Wu, 1982).

The Small-Scale and Large-Scale Components of Wave-Train Energy

Approach to Modeling the Small-Scale Component

In general, topographic scattering is most significant when the wavelength of the incident wave is comparable to the scale of the roughness. Four models are calculated with different Gaussian-type random topographies marked in Figure 11. Each total energy curve is decomposed into a small-scale component (high-frequency fluctuations) and a large-scale component (low-frequency tendency). Figure 11 shows the comparison between the random topographic

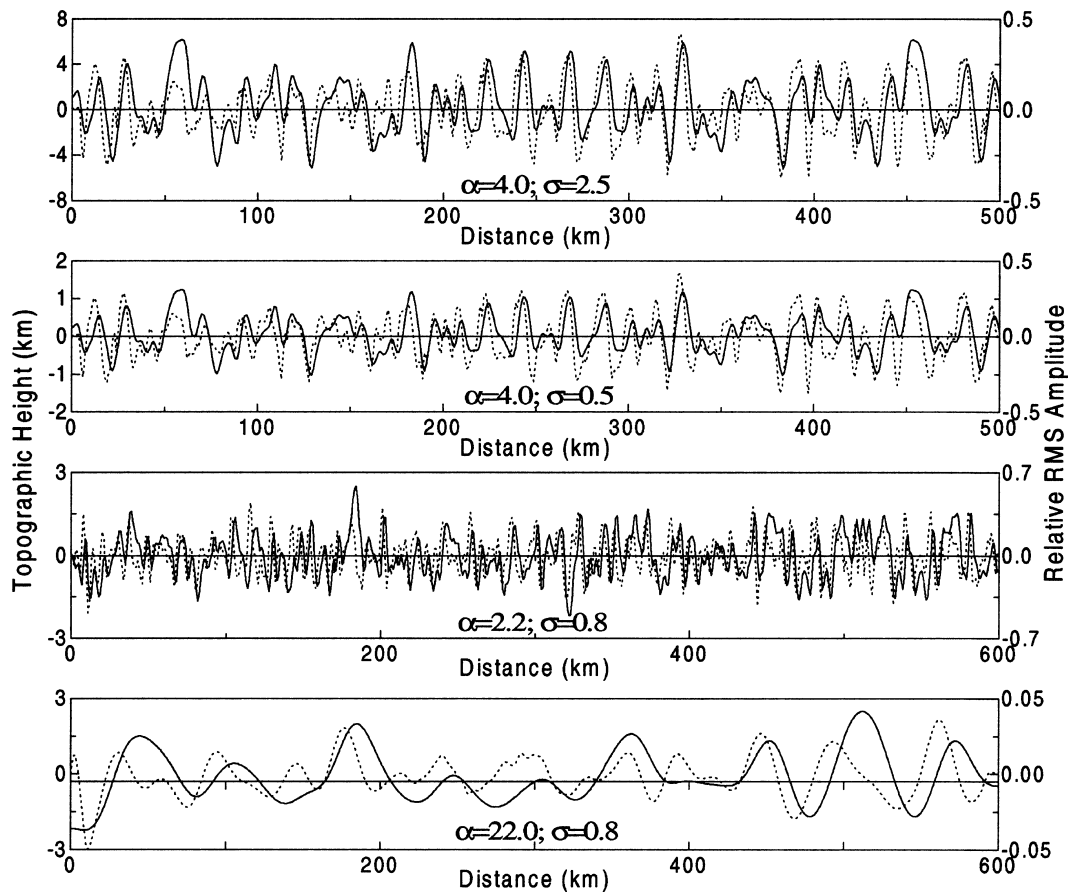


Figure 11. Comparison between the topographic curve (solid line) and the small-scale components (dotted line) of the corresponding energy profile. From top to bottom, four topographic models are used with different roughness of the correlation length a and the surface rms height σ .

curve (solid line) and the small-scale component (dotted line) of the computed total energy curve versus distance.

We see that for all the models, the small-scale energy profiles show strong similarity with random topographic curves. Especially for the upper three models, the fit of the solid with the dotted lines is better than that in the bottom model where the surface correlation length a increases to 22 km. The correlation between these two types of curves is further depicted in Figure 12, where the cross-correlation function between the topography curve and the small-scale component of energy curve for each model is plotted as a function of shift. The correlation coefficients for these four cases presented in Figure 11 reach up to 0.766, 0.765, 0.706, and 0.638, respectively. The reason for the bad fit in the bottom model lies probably in the sensitivity of wavelength to roughness scales, that is, the dominant frequency of the source wavelet chosen for simulation appears to be much smaller than the topographic scale. The contribution of topographic scattering to the variation of energy curve comes mainly from the wave-field component with its wavelength comparable to the topographic scales.

Figure 11 also illustrates that rough surface structures

remove some energy from the specular direction and lead to energy attenuation of regional phases. An important fact exposed by the small-scale energy profile is that the constructive/destructive interference in a local topographic structure has a short range of action. The effect extends only to the neighborhood of a number of surface-scattering points. Bouchon (1973) and Boor (1973) have noted that convex topographic features usually cause larger amplifications than concave topography. The energy curves in Figure 11 show that energy focusing occurs at the convex surfaces, while energy defocusing occurs at the concave surfaces. Relating individual variations in the energy curves in Figure 11 to the local geometric features in the topographic curves reveals the dependence of amplification on the ratios of height-to-half-width of a convex. This amplification pattern was clearly demonstrated by Bouchon *et al.* (1996). They used a semianalytical, seminumerical method to investigate the effect of a 3D hill on ground motion and confirmed that amplification occurs near the top of the hill. Sensors in the summit area of convex topography will detect prominent arrivals due to the scattered energy trapped within the hills. Topographic amplification, sometimes quite big, is consid-

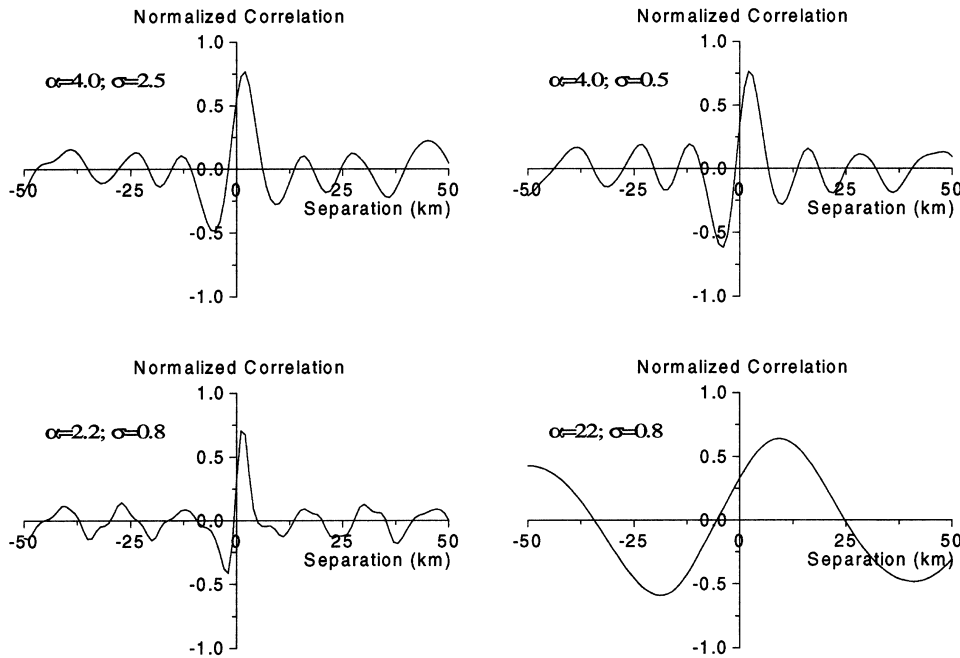


Figure 12. Cross-correlation function of the topographic curve with the small-scale energy components, plotted as a function of separation. Four graphs with different roughness parameters (a and σ) correspond to those presented on Figure 11.

erably complex and hard to estimate from the information of topographic geometry (see Fig. 11). The evaluation of amplification has been conducted by many researchers (e.g., Sauchez-Sesma and Campillo, 1993) for relatively simple topographies. For arbitrarily irregular topographies, the level of amplification may be statistically estimated, as implied by this study. The numerical calculations, however, often systematically underestimate the actual amplifications observed in the field (e.g., Geli *et al.*, 1988). Amplification is currently assumed to depend on the ratios of height-to-half-width of a hill and the local angles of incidence. The two factors, however, for a rough surface, will vary along the surface, depending on the local surface gradient.

Approach to Modeling the Large-Scale Component

If topographic properties are described by statistical approaches, the scattered field from a random topography will itself be random and can be characterized by statistical parameters. Scattering attenuation is represented by the large-scale component of the energy curve. It is characterized by an exponential decay and may be expressed by a scattering Q that is implicitly associated with topographic statistics. The analysis of spatial attenuation of Lg waves can be approached by a number of approximate solutions depending on the complexity of the problem. The attenuation mechanisms involved with Lg waves include anelastic absorption, scattering, geometrical spreading, and leakage to the mantle. For stable continental areas, Campillo (1990) pointed out that the major characteristics of Lg might be well understood in terms of wave propagation in standard flat-layered crustal

models. The quality factor of Lg in the group velocity window $3.5\text{--}2.8 \text{ km sec}^{-1}$ may be computed from the observed decay of amplitude with epicentral distance if the geometrical attenuation of the phase can be evaluated theoretically. In our homogeneous wave guides, the distance-dependent attenuation of guided waves includes backscattering, geometrical spreading, and Moho leakage.

In our homogeneous wave guides with rough topographies, the decay of the guided wave energy with distance from an initial energy $E(x_0)$ at a near-source receiver x_0 can be modeled as

$$E(x) = E(x_0)G(x)\exp(-\eta x), \quad (5)$$

where x is the epicentral distance, $G(x)$ represents the geometric factor, and η is a constant that represents the apparent attenuation coefficient for guided crustal waves. In this study, we use two steps to evaluate scattering Q . First, using least-squares fits, we compute the geometrical attenuation of Lg for the reference wave guide in the absence of topographic scattering. Second, the scattering effects from rough topographic waveguides can be regarded as a deviation from the reference wave guide, and equation (5) is used to extract apparent attenuation coefficients from the decay of Lg energy with distance.

Figure 13 shows the energy attenuation for the reference wave guide with its critical distance around 90 km. The dotted line is the best fit to the energy curve. It denotes a combined attenuation of the geometrical spreading and the Moho

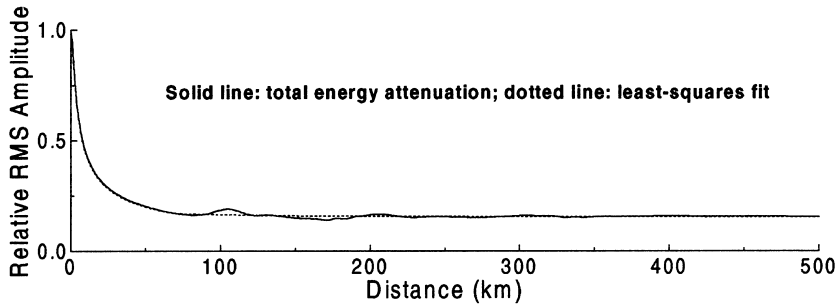


Figure 13. Total energy attenuation versus distance for the reference wave guide. The dotted line is the best fit to the data by the geometric spreading $G(x)$ in equation (6).

penetration before critical angle, computed by least-squares fits:

$$G(x) = \begin{cases} x^{-0.5}/x_0^{-0.5}, & x < 90 \text{ km} \\ x^{-1}/x_0^{-0.5}, & x > 90 \text{ km} \end{cases} \quad (6)$$

The fitting of the energy curve has to be separated into two parts (i.e., precritical and postcritical distances) because of their different behaviors of wave propagation. Within the precritical distance, a considerable portion of energy with steep angles is removed because of the Moho penetration. The attenuation reduces after passing the critical distance, and the energy becomes constant with distance. Clearly, equation (6) is a good approximation to the reference wave guide.

In the second step, we change the flat free surface of the reference wave guide into a randomly rough surface. Two random topographies with the same scale length ($ka = 7.18$) but different surface rms heights, (one with $\sigma = 0.5$ and another with $\sigma = 2.5$) are used in the scattering Q evaluation. Figure 14 gives the attenuation curves (thick line) for these two random topographies. Stronger attenuation is as expected with $\sigma = 2.5$. The large-scale trends of the energy profiles can be fitted into the exponential pattern in equation (5) by least-square fits. Due to the reason mentioned in the previous paragraph, the scatter of the data in the pre-critical distance less than 100 km is large. Beyond the critical distance, the attenuation curve fits well with the exponential law. The scattering Q values measured from the exponential decay curves are 786 for $\sigma = 0.5$ and 197 for $\sigma = 2.5$.

Figure 14 illustrates that the large-scale energy component is representative of spatial attenuation of Lg waves caused by topographic scattering. The topographic scattering Q measured by the large-scale component is strongly dependent on both the surface correlation length and the surface rms height. More detailed investigation on topographic scattering Q from the decay of Lg amplitude with distance is discussed through numerical simulation in the next section.

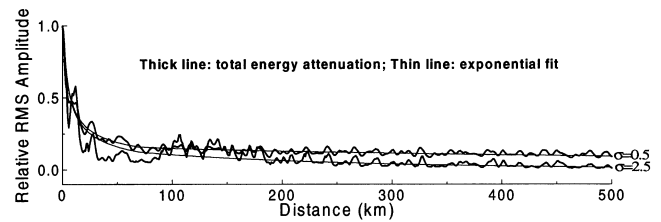


Figure 14. Total energy attenuation versus distance for two topographic models (see Fig. 4). The exponential fit is calculated using equation (5) with $G(x)$ given by Figure 13.

Energy Attenuation in Wave Guides with Random Topography

Although topography statistics have been known empirically to affect regional wave propagation, there is a lack of understanding on why and how they works. It is often difficult to separate topographic scattering attenuation from other attenuation mechanisms (e.g., intrinsic attenuation, Moho leakage, and scattering attenuation by small-scale volume heterogeneities) along the propagation path. However, numerical simulation can offer some help in solving this problem. In this section, the Lg attenuation mechanism by randomly rough topographies is further studied based on synthetics. We use the two-step analysis method described in the last section to study the relation of the apparent inverse quality factor Q^{-1} and the scale length ka of a random topography, where $k = 2\pi/\lambda_0$ and λ_0 is the dominant wavelength of the incident wave. We vary a but fix σ in order to relate scattering attenuation to the dimensionless length ka . In our numerical modeling, we use three different topographies: the reference wave guide with a flat surface, the large- a wave guide with $a = 22$, and the small- a wave guide with $a = 2.2$. The topographic curves for the latter two wave guides are shown in Figure 9. For each wave guide, synthetic seismograms observed along the topography are computed for all the cases listed in Table 1. Here a case means a computer run of a model. The wavelet dominant frequency f_0 and the frequency range computed are different for each case, corresponding to different ka value. The total energy attenuation curve is calculated against distance from the synthetic seismograms for each case.

Table 1

The Wavelet Dominant Frequency f_0 and Computed Frequency Range for All the Cases

Case*	f_0 (Hz)	Band (Hz)
1	0.2	0.0–1.0
2	0.5	0.0–1.0
3	0.7	0.0–1.4
4	1	0.0–2.0
5	1.3	0.0–2.4
6	1.6	0.0–2.8
7	2	0.0–3.4
8	2.3	0.0–4.0
9	2.6	0.0–4.5
10	3	0.0–5.4
11	3.5	0.0–6.4
12	4	0.0–7.4

*Computer run of the model.

Figure 15 presents the curved surfaces of energy attenuation against distance and frequency in a 3D plot, from top to bottom, corresponding to the reference wave guide, large- a wave guide, and small- a wave guide, respectively. We see that the energy partition and attenuation due to topographic scattering depend very strongly on frequency and the characteristic scales of random topographies. The energy surface for the reference wave guide is quite flat. This provides a proper ground to identify the deviation caused by topographic-scattering attenuation. Large changes occur in the energy surface of the small- a waveguide where the surface gradient varies dramatically along both the frequency and the distance axes. As expected, the maximum attenuation is at the vicinity of the characteristic frequency. An unexpected problem in this energy surface is that there appears to be more than one energy minimum concave along the frequency axis when propagating beyond about 400 km.

It should be noted that the attenuation surface of total energy presented in Figure 15 is the energy contained in the whole seismogram recorded on the surface, that is, it includes the Lg coda. The built-up energy by forward and backscattering along the path partly contributes to the Lg coda and partly leaks to the mantle. The topographic-scattering-driven leakage is the only source of wave-train energy loss in our examples. The two-step energy analysis method is employed to fit the total energy attenuation for each case in order to evaluate the Moho leakage loss due to the topographic scattering. The results are shown in Figure 16 for the large- a wave guide and in Figure 17 for the small- a wave guide. We see that equation (6) fits the energy of the reference wave guide well for all the cases. This provides a proper $G(x)$ evaluation accounting for the geometrical spreading and the Moho leakage in the reference wave guide during the Lg -formation process. Given $G(x)$, equation (5) appears to fit the energy curves excellently for both the large- a and small- a wave guides in each case, especially at distances beyond the critical distance. The apparent attenuation coefficient η and the apparent inverse quality factor Q^{-1} are

calculated for all the cases and plotted in Figure 18 as functions of wavelength and frequency, respectively.

Note that enhanced attenuation occurs over a limited range of frequencies around 0.5–1.5 Hz for the small- a wave guide and 1.0–2.0 for the large- a wave guide, in which the trapped energy for both the cases generally remains fairly stable with less frequency sensitivity. In the range of higher or lower frequencies, the topographic scattering attenuation becomes weak. As expected, the scattering attenuation in the small- a wave guide is stronger than in the large- a wave guide. The frequency dependence of topographic scattering Q is demonstrated in the figure for the large- a and small- a wave guides, which is found to be modeled as $Q = Q_0 f^n$, where n describes the frequency dependence of Q . The exponent n is strongly related to the tectonic features of the region of Lg propagation and has been widely used as a continental index (e.g., Nuttli, 1973; Mitchell, 1980; Sato, 1984; Campillo *et al.*, 1985; Xie, 1993; McNamara *et al.*, 1996). For example, Campillo *et al.* (1985) combined data analysis and numerical modelling to give $Q = 290f^{0.52}$ for the crust beneath central France. McNamara *et al.* (1996) found $Lg Q = (366 \pm 37)f^{(0.45 \pm 0.06)}$ for event/station paths confined to the Tibetan Plateau. Stable regions such as eastern North America are characteristic of lower values (Mitchell, 1980). A least-squares fit to the curve $Q^{-1} - f$ in Figure 18 gives $Q = 269 f^{0.44}$ for the small- a wave guide and $Q = 764f^{0.2}$ for the large- a wave guide. From these comparisons, we may conclude that the levels of Lg attenuation caused only by topographic scattering in these two scales are comparable to those observed in some regions.

Figure 19 shows the apparent inverse quality factor Q^{-1} plotted against the dimensionless scale length ka for the small- a and large- a wave guides. We see that Q^{-1} at its peak value of -1.9 around $ka \approx 0.8$ – 1.0 in the small- a wave guide decreases gradually until $ka \approx 2.0$ and then reduces rapidly to the value of -3.0 at $ka = 10.0$. As pointed out by Wu (1982), for backscattering, the maximum scattering Q^{-1} is around $ka = 1.0$ and decreases rapidly after $ka > 1.0$, whereas for large-angle forescattering, the plateau with high Q^{-1} is quite wide after $ka = 1.0$. Like volume-scattering attenuation, topographic scattering is also an apparent attenuation. The energy is redistributed by scattering along the rough surface that progressively shifts energy off the specular direction. The portion with large-angle waves tends to leak into the mantle and causes energy loss. The scale-dependent behavior of Q^{-1} in Figure 19 might imply that the Moho leakage loss due to topographic scattering in the small- a wave guide results largely from the backscattering with large angles. Unexpectedly, Q^{-1} seems to reach its second peak around $ka \approx 25.0$ – 40.0 with a wide plateau in the large- a waveguide. The slow decrease of Q^{-1} with ka indicates the feature of large-angle forescattering dominance in the large- a wave guides. Here we only model two correlation lengths with $a = 2.2$ and $a = 22$, which cannot provide a complete description of scattering attenuation Q^{-1} along the ka axis. The earth's surface generally has multiple-

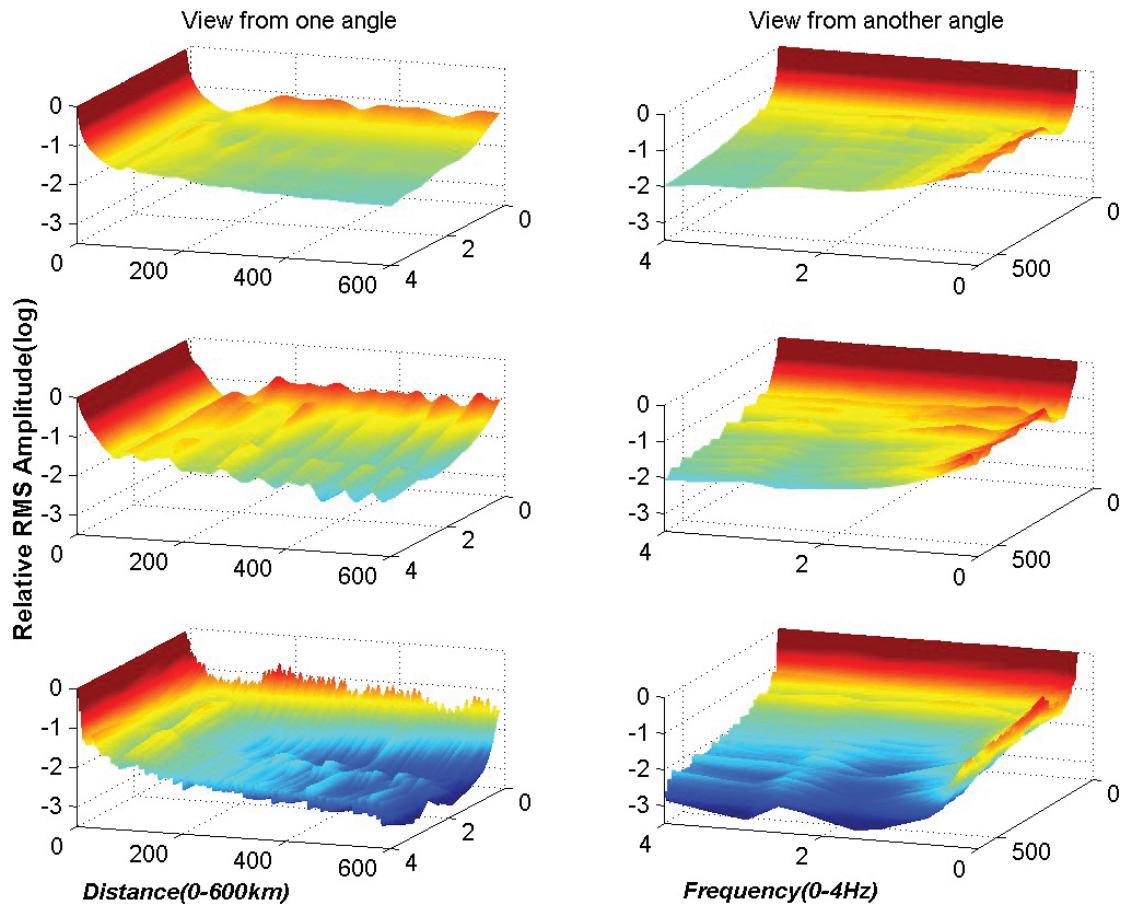


Figure 15. Energy attenuation surface versus distance and frequency. From top to bottom, the reference wave guide, the large- a wave guide, and the small- a wave guide.

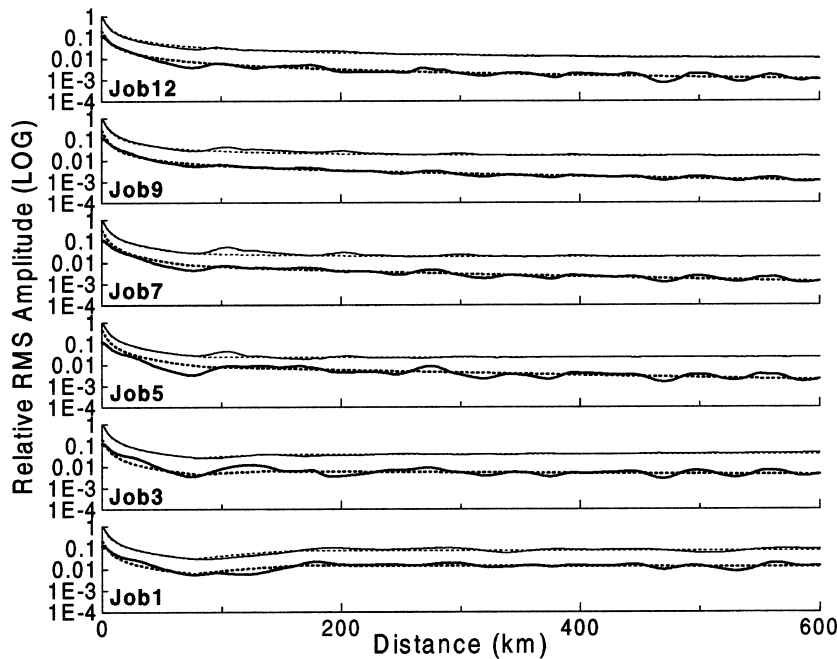


Figure 16. Least-squares fitting of the total energy attenuation for each case in the large- a waveguide. First, the energy (thin solid) of the reference wave guide is fitted by equation (6) to produce $G(x)$ (thin dotted line). Then equation (5) is used for the energy (thick solid) of the large- a waveguide to produce an exponential fitting curve (thick dotted line).

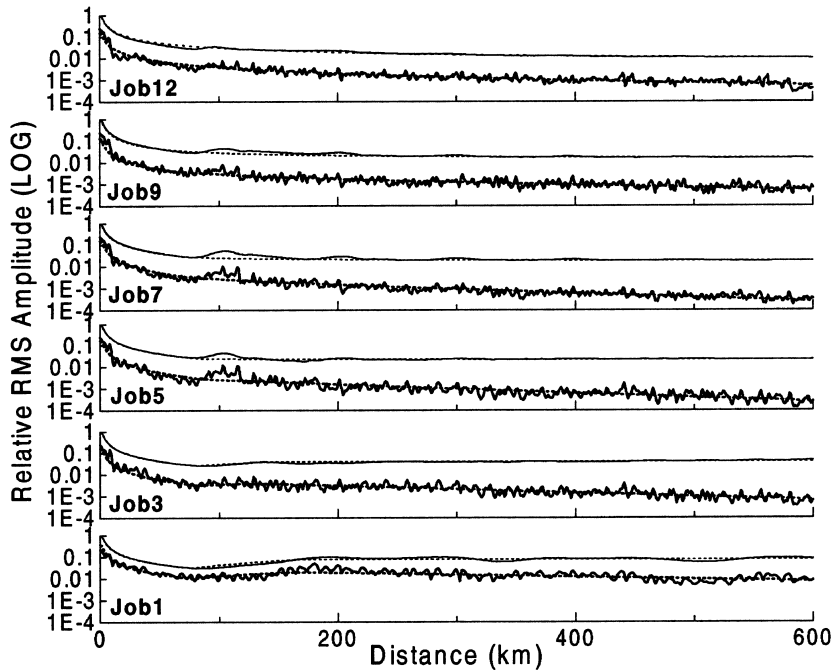


Figure 17. Least-squares fitting of the total energy attenuation for each case in the small- a wave guide. First, the energy (thin solid) of the reference wave guide is fitted by equation (6) to produce $G(x)$ (thin dotted line). Then equation (5) is used for the energy (thick solid) of the small- a wave guide to produce an exponential fitting curve (thick dotted line).

scale inhomogeneities that complicate the frequency- and ka -dependent relations of topographic scattering attenuation Q^{-1} . These relations are very path-dependent due to scattering sensitivity to characteristic scales of rough topographies encountered by propagation. Numerical experiments combined with analytic studies need to be conducted in the future for more complete assessment of the frequency- and ka -dependent behavior of topographic scattering Q^{-1} for regional phases.

Conclusion and Discussion

The efficient propagation of Lg up to a few thousand kilometers is associated with its mode of multiple, supercritical reflections (Bouchon, 1982) in the crust, largely between the Moho and free surface. Strong attenuation and blockage of Lg are related to the disruption of the propagation mode. Numerical modeling is used in this study to identify the topographic scattering characteristics with respect to regional phases. We investigate the spatial pattern of distance-dependent variations of the wave-train energy caused by topographic scattering along the path and aim to characterize its scale-dependent relations with topographic statistics. The study strengthens the concept that topographic scattering might be a powerful mechanism to attenuate regional waves. The main conclusions can be summarized as follows:

1. The topographic-scattering-driven energy distribution over a long distance is usually characteristic of an atten-

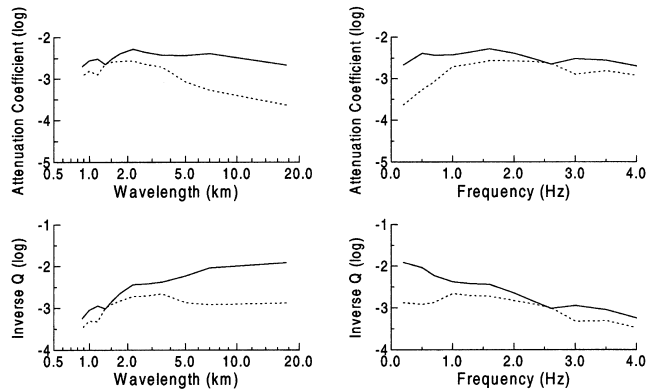


Figure 18. Apparent attenuation coefficient and apparent inverse quality factor as a function of wavelength and frequency, respectively. The solid line for the small- a wave guide can be fitted by the functional relationship $Q = 269f^{0.44}$. The dotted line for the large- a wave guide can be fitted by $Q = 764f^{0.2}$.

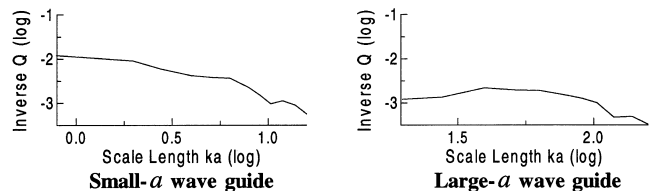


Figure 19. Apparent inverse quality factor as a function of the scale length ka from the small- a wave guide (left panel) and the large- a wave guide (right panel).

- uation trend on the long-distance scale accompanied by amplitude fluctuations on the smaller-distance scales. The energy curve can be divided meaningfully into small-scale and large-scale components that are correlated with along-path topographic statistics in quite different manners.
- The small-scale energy component, leading to anomalous waveform distortions in the time domain, is strongly related to the near-receiver topographic geometry. The small-scale energy curve has a striking similarity to the corresponding topographic curve. The fluctuation of amplitude is mainly related to the surface rms height σ , the wavelength of the incident wave, and the local incident angles.
 - Topographic scattering attenuation is represented by the large-scale energy component on the long-distance behavior of the scattering surface. For a trapped mode, the component can be described by a topographic scattering Q . The topographic scattering Q is dependent on the surface rms height σ , the surface correlation length a , and the wavelength of the incident wave.
 - A two-step analysis method is presented to evaluate the leakage loss due to topographic diffusion scattering. Numerical simulations (see Table 1) have found $Lg Q = 269f^{0.44}$ for the small- a wave guide and $Q = 764f^{0.2}$ for the large- a wave guide. These are comparable with some observations with Q measured as a mean value in the crust. More quantitative assessment of the frequency- and ka -dependent behavior of topographic scattering Q^{-1} for regional phases needs to be conducted in the future.

Acknowledgments

We thank Dr. K. Yoshimoto for his helpful discussions about the algorithm of random medium generation. Part of this research was carried out when L.Y.F worked at UCSC, supported by the Department of Energy through Contract F19628-95-K-0016 (administered by the Phillips Laboratory of the Air Force) and by the Defense Special Weapons Agency through Contract DSWA01-97-1-0004.

References

- Baumgardt, D. R. (1990). Investigation of teleseismic Lg blockage and scattering using regional arrays, *Bull. Seism. Soc. Am.* **80**, 2261–2281.
- Baumgardt, D. R., and D. Der (1994). Investigation of the transportability of the P/S ratio discriminant to different tectonic regions, Scientific Report No. 1, PL-TR-94-2299. ENSCO, Inc., Springfield, Virginia.
- Boore, D. (1973). The effect of simple topography on seismic waves: implications for the accelerations recorded at Pacoima Dam, San Fernando Valley, California, *Bull. Seism. Soc. Am.* **63**, 1603–1609.
- Bouchon, M. (1973). Effect of topography on surface motion, *Bull. Seism. Soc. Am.* **63**, 615–632.
- Bouchon, M. (1982). The complete synthesis of seismic crustal phases at regional distances, *J. Geophys. Res.* **82**, 1735–1741.
- Bouchon, M., C. A. Schultz, and M. N. Toksöz (1995). A fast implementation of boundary integral equation methods to calculate the propagation of seismic waves in laterally varying layered media, *Bull. Seism. Soc. Am.* **85**, 1679–1687.
- Bouchon, M., C. A. Schultz, and M. N. Toksöz (1996). Effect of three-dimensional topography on seismic motion, *J. Geophys. Res.* **101**, 5835–5846.
- Campillo, M. (1987). Lg wave propagation in a laterally varying crust and the distribution of the apparent quality factor in Central France, *J. Geophys. Res.* **92**, 12,604–12,614.
- Campillo, M. (1990). Propagation and attenuation characteristics of the crustal phase Lg, *Pure Appl. Geophys.* **132**, 1–19.
- Campillo, M., B. Feignier, M. Bouchon, and N. Bethoux (1993). Attenuation of crustal waves across the Alpine range, *J. Geophys. Res.* **98**, 1987–1996.
- Campillo, M., J. L. Plantet, and M. Bouchon (1985). Frequency-dependent attenuation in the crust beneath central France from Lg waves: data analysis and numerical modeling, *Bull. Seism. Soc. Am.* **75**, 1395–1411.
- Chen, X. F. (1995). Seismogram synthesis for multi-layered media with irregular interfaces by the global generalized reflection/transmission matrices method II. Applications of 2-D SH case, *Bull. Seism. Soc. Am.* **85**, 1094–1106.
- Dravinski, M. (1982). Influence of interface depth upon strong ground motion, *Bull. Seism. Soc. Am.* **72**, 597–614.
- Fan, G., and T. Lay (1998). Statistical analysis of irregular wave-guide influence on regional seismic discriminants in China, *Bull. Seism. Soc. Am.* **88**, 74–88.
- Frankel, A., and W. Leith (1992). Evaluation of topographic effects on P and S-waves of explosions at the northern Novaya Zemlya test site using 3-D numerical simulations, *Geophys. Res. Lett.* **19**, 1887–1890.
- Fu, L. Y. (1996). 3-D boundary element seismic modeling in complex geology, in *66th Annual International Meeting Soc. Expl. Geophys.*, Denver, Colorado, USA, 10–15 November, Expanded Abstracts, 1239–1242.
- Fu, L. Y., and Y. G. Mu (1994). Boundary element method for elastic wave forward modeling, *Acta Geophys. Sinica* **37**, 521–529.
- Fu, L. Y., and R. S. Wu (2000). Infinite element-based absorbing boundary technique for elastic wave modeling, *Geophysics* **62**, 596–602.
- Fu, L. Y., and R. S. Wu (2001). A hybrid BE-GS method for modeling regional wave propagation, *Pure Appl. Geophys.* **158**, 1251–1277.
- Geli, L., P. Y. Bard, and B. Jullien (1988). The effect of topography on earthquake ground motion: a review and new results, *Bull. Seism. Soc. Am.* **78**, 42–63.
- Gibson, R. L., Jr., and M. Campillo (1994). Numerical simulation of high- and low-frequency Lg-wave propagation, *Geophys. J. Int.* **118**, 47–56.
- Hartse, H., R. Flores, and P. Johnson (1998). Correcting regional seismic discriminants for path effects in western China, *Bull. Seism. Soc. Am.* **88**, 596–608.
- Hudson J. A., R. F. Humphries, I. M. Mason, and V. K. Kambhavi (1973). The scattering of longitudinal elastic waves at a rough free surface, *J. Phys. D. Appl. Phys.* **6**, 2174–2186.
- Jih, R. S. (1996). Waveguide effects of large-scale structural variation, anelastic attenuation, and random heterogeneity on SV Lg propagation: a finite-difference modeling study, in *Proc. 18th Annual Seismic Research Symposium on Monitoring a Comprehensive Test-Ban Treaty*, Annapolis, Maryland, USA, 4–6 September, 182–194.
- Kadinsky-Cade, K., M. Barazangi, J. Oliver, and B. Isacks (1981). Lateral variations of high-frequency seismic wave propagation at regional distances across the Turkish and Iranian Plateau, *J. Geophys. Res.* **86**, 9377–9396.
- Kennett, B. L. N. (1972). Seismic waves in laterally varying media, *Geophys. J. R. Astr. Soc.* **27**, 310–325.
- Kennett, B. L. N. (1984). Guided wave propagation in laterally varying media. I. Theoretical development, *Geophys. J. R. Astr. Soc.* **79**, 235–255.
- Kennett, B. L. N. (1986). Lg waves and structural boundaries, *Bull. Seism. Soc. Am.* **76**, 1133–1141.
- Kennett, B. L. N. (1989). On the nature of regional seismic phases-I. Phase representations for Pn, Pg, Sn, Lg, *Geophysical Journal*, **98**, 447–456.
- Kennett, B. L. N. (1998). Guided waves in three-dimensional structures, *Geophys. J. Int.* **133**, 159–174.

- Maupin, V. (1989). Numerical modeling of Lg wave propagation across the North Sea central graben, *Geophys. J. Int.* **99**, 273–283.
- McLaughlin, K. L., and R. S. Jih (1988). Scattering from near-source topography: Teleseismic observations and numerical simulations, *Bull. Seism. Soc. Am.* **78**, 1399–1414.
- McNamara, D. E., T. J. Owens, and W. R. Walter (1996). Propagation characteristics of Lg across the Tibetan plateau, *Bull. Seism. Soc. Am.* **86**, 457–469.
- Mitchell, B. J. (1980). Frequency dependence of shear wave internal friction in the continental crust of Eastern North America, *J. Geophys. Res.* **85**, 5212–5218.
- Ni, J., and M. Barazangi (1983). High-frequency seismic wave propagation beneath the Indian Shield, Himalayan Arc, Tibetan Plateau and surrounding regions: high uppermost mantle velocities and efficient Sn propagation beneath Tibet, *Geophys. J. R. Astr. Soc.* **72**, 665–689.
- Nuttli, O. W. (1973). Seismic wave attenuation and magnitude relations for eastern north America, *J. Geophys. Res.* **78**, 876–885.
- Ogilvy, J. A. (1991). *Theory of wave scattering from random rough surfaces*, A. Hilger, Bristol, England.
- Rodgers, A., T. Lay, G. Fan, and W. Walter (1997). Calibration of distance and path effects on regional P/S discriminants at station ABKT (Alibek, Turkmenistan): statistical analysis of crustal waveguide effects. Lawrence Livermore National Laboratory, UCRL-JC-129165.
- Ruzaikin, A. L., I. L. Nersesov, V. I. Khalaturin, and P. Molnar, P. (1977). Propagation of Lg and lateral variations in crustal structure in Asia, *J. Geophys. Res.* **82**, 307–316.
- Sanchez-Sesma, F. J., and M. Campillo (1991). Diffraction of P, SV and Rayleigh waves by topographic features: a boundary integral formulation, *Bull. Seism. Soc. Am.* **81**, 2234–2253.
- Sanchez-Sesma, F. J., and M. Campillo (1993). Topographic effects for incident P, SV and Rayleigh waves, *Tectonophysics* **218**, 113–125.
- Sato, H. (1984). Attenuation and envelope formation of three-component seismograms of small local earthquakes in randomly inhomogeneous lithosphere, *J. Geophys. Res.* **89**, 1221–1241.
- Sato, H., and M. C. Fehler (1998). *Seismic Wave Propagation and Scattering in the Heterogeneous Earth*, Springer, New York.
- Trifunac, M. D. (1973). Scattering of plane SH-waves by a semi-cylindrical canyon, *Earthquake Eng. Struct. Dyn.* **1**, 267–281.
- Wong, H. L., and P. C. Jennings (1975). Effect of canyon topographics on strong ground motion, *Bull. Seism. Soc. Am.* **65**, 1239–1257.
- Wu, R. S. (1982). Attenuation of short period seismic waves due to scattering, *Geophys. Res. Lett.* **9**, 9–12.
- Wu, R. S. (1985) Multiple scattering and energy transfer of seismic waves: separation of scattering effect from intrinsic attenuation. I. Theoretical modelling, *Geophys. J. R. Astr. Soc.* **82**, 57–80.
- Wu, R. S., X. B. Xie, and X. Y. Wu (1999). Lg wave simulations in heterogeneous crusts with irregular topography using half-space screen propagators, in *Proc. 21th Annual Seismic Research Symposium on Monitoring a Comprehensive Test-Ban Treaty*, 683–693.
- Wu, R. S., S. Jin, and X. B. Xie (1996). Synthetic seismograms in heterogeneous crustal waveguides using screen propagators, in *Proc. 18th Annual Seismic Research Symposium on Monitoring a Comprehensive Test-Ban Treaty*, Annapolis, Maryland, USA, 4–6 September, 290–300.
- Wu, R.S., S. Jin, and X. B. Xie (2000a). Seismic wave propagation and scattering in heterogeneous crustal waveguides using screen propagators. I. SH waves, *Bull. Seis. Soc. Am.* **90**, 401–413.
- Wu, R. S., S. Jin, and X. B. Xie (2000b). Energy partition and attenuation of Lg waves by numerical simulations using screen propagators, *Phys. Earth Planet. Inter.* **120**, 227–244.
- Xie, J. (1993). Simultaneous inversion for source spectrum and path Q using Lg with application to three Semipalatinsk explosions, *Bull. Seism. Soc. Am.* **83**, 1547–1562.
- Zhang, T. and T. Lay (1994). Analysis of short-period regional phase path effects associated with topography in Eurasia, *Bull. Seism. Soc. Am.* **84**, 119–132.
- Zhang, T., T. Lay, S. Schwartz, and W. R. Walter (1996). Variation of regional seismic discriminants with surface topographic roughness in the Western United States, *Bull. Seism. Soc. Am.* **86**, 714–725.
- Commonwealth Scientific and Industrial Research Organization
P. O. Box 1130
Bentley, WA 6102, Australia
Li-Yun.Fu@csiro.au
(L.-Y.F.)
- Institute of Geophysics and Planetary Physics
University of California
1156 High Street, Santa Cruz, California 95064
wrs@es.ucsc.edu
(R.-S.W.)
- Laboratoire de Géophysique Interne et Tectonophysique
Université Joseph Fourier
BP53X, 38041, Grenoble Cedex, France
(M.C.)

Manuscript received 15 December 2000.